Impact Analysis of Fast Dynamics on Stability of Grid-Tied Inverter Based on Oscillator Model and Damping Torque Analysis

Pan Yu, Zhen Tian, *Member, IEEE*, Xiaoming Zha, *Member, IEEE*, Jianjun Sun, *Member, IEEE*, Peijun Zhong, and Meng Huang, *Member, IEEE*

***Abstract*—As the crucial interface of renewable energy integration, the grid-tied inverter is a complicated system with a multi-timescale feature, containing both fast dynamics and slow dynamics that determine the system stability. However, previous researches on stability analysis mainly focus on the slow dynamics without considering the impact of fast dynamics, which may bring to inaccurate stability prediction. In this paper, the impact of fast dynamics on stability is investigated for grid-tied inverter from a physical perspective. Considering the dynamics of the current control loop and network, a two degrees-of-freedom oscillator model is firstly established to extract the fast dynamics separately. The damping torque analysis is then applied to analyze the impact of the extracted fast dynamics on the damping and spring coefficients of slow dynamics. Moreover, based on the fast dynamic analysis, a novel reduced-order model is proposed with the consideration of the dominant characteristics of fast dynamics, which improves the model accuracy without increasing the complexity. Eventually, both numerical evaluations and experiments are performed to validate the proposed analysis method.**

***Index Terms*—Grid-tied inverter, fast dynamics, small-signal stability, oscillator model, damping torque analysis.**

I. Introduction

AS THE most crucial interface of renewable energy integration, grid-tied inverters greatly affect the stability of modern power systems with high penetration of renewable energy [1], [2]. In recent years, the oscillation problems related to inverters have been reported continuously [3]–[6], which poses a huge threat to the stable operation of power systems integrated with renewable energy. In order to propose specific solutions, it is a prerequisite to reveal the mechanism of oscillatory instability of inverters.Grid-tied inverters are typical multi-timescale systems because of the significant difference in the bandwidth of its multiple control loops [7]. The current control loop and network dynamic are divided into fast dynamics, while the dc-link voltage control loop, phase-locked loop (PLL), and other outer controllers are divided into slow dynamics [8]. Therefore, system stability is determined by both the fast and slow dynamics of the grid-tied inverter.

Previous studies mainly attribute the origin of instability to the slow dynamics, and the modal analysis or impedance-based analysis is widely used to investigate the stability of the grid-tied inverter [9]–[11]. However, these analyses based on the detailed inverter model are too complicated to assess the interaction effect within the internal control loops. In order to develop insight into the stability of grid-tie inverters, the interaction between slow dynamics is analyzed in [12]–[14] by ignoring fast dynamics, while the high-frequency instability phenomenon induced by fast dynamics is investigated in [15] without considering slow dynamics. These studies are helpful to reveal the instability mechanism of the inverter at a specific timescale, but the analysis of arbitrarily ignoring fast or slow dynamics is inevitable inaccurate since the fast and slow dynamics interact with each other. In [16] and [17], it is found that the fast dynamics of the current control loop and network dynamics have a significant impact on the slow dynamics of the outer control loop. It means that the interaction analysis between fast and slow dynamics is important for the inverter stability assessment, but this issue has not yet been extensively investigated.

On the other hand, for the stability analysis of power systems integrated with large-scale inverters, it has been reported in [6] and [18] that the potential resonance may occur between the inverter and the synchronous generator. It implies that the inverter stability dominated by slow dynamics should deserve more attention. From this perspective, in the interaction analysis between fast and slow dynamics, the impact of fast dynamics on the instability phenomenon of the inverter caused by slow dynamics is more worthy of exploration. The interaction between PLL and fast dynamics during low-voltage ride through is analyzed in [19], it is revealed that the fast dynamics may reduce the PLL damping, which deteriorates the stability of the inverter. However, it is not clear how each component of fast dynamics affects the system stability since all fast dynamics are regarded as a sub-system, and the dc-link voltage control loop is not included in the analysis. Thus, the impact of the fast dynamics on system stability still needs to be further explored.

Manuscript received December 18, 2020; revised April 12, 2021 and July 6, 2021; accepted September 2, 2021. Date of publication September 8, 2021; date of current version April 19, 2022. This work was supported by the National Natural Science Foundation of China under Grants U1866601, 51637007, 51777145, and 52007134. Paper no. TPWRS-02070-2020. *(Corresponding author: Xiaoming Zha.)*

The authors are with the School of Electrical Engineering and Automation, Wuhan University, Wuhan 430072, China (e-mail: pyu@whu.edu.cn; tianzhenctrl@126.com; xmzha@whu.edu.cn; jjsun@whu.edu.cn; pjzhong@whu.edu.cn; meng.huang@whu.edu.cn).

Color versions of one or more figures in this article are available at https://doi.org/10.1109/TPWRS.2021.3110863.

Digital Object Identifier 10.1109/TPWRS.2021.3110863

0885-8950 © 2021 IEEE. Personal use is permitted, but republication/redistribution requires IEEE permission.
See https://www.ieee.org/publications/rights/index.html for more information.

Authorized licensed use limited to: SICHUAN UNIVERSITY. Downloaded on June 06,2022 at 09:26:40 UTC from IEEE Xplore. Restrictions apply.

Moreover, a reduced-order model that preserves the dominant characteristics of inverters is important for the control and stability analysis of power systems [8]. The conventional model reduction intuitively discards states with fast dynamics [20], [21]. But as mentioned above, fast dynamics also affect the inverter stability, the component of fast dynamics which has a great influence on the system should be preserved. In [8], the modal truncation method is applied to reduce the model order, the interaction between fast and slow dynamics was taken into account, whereas the physical meaning of the order reduction is not clear. In addition, some complex algorithms are used for model reduction [22], [23], but the methods are too complicated.

In order to cover the aforementioned insufficient, this study investigates the impact of fast dynamics on inverter stability dominated by slow dynamics, and then a novel reduced-order model that retains the main feature of fast dynamics is proposed. The main contributions of this paper are summarized as follows:

1) A two degrees-of-freedom oscillator model is established based on the detailed small-signal model of the grid-tied inverter, which separately extracts the fast dynamics from the complicated mathematical models.
2) The damping torque analysis is adopted to decompose the contribution of fast dynamics to the system as the additional damping and spring terms, which quantifies the impact of fast dynamics on inverter stability.
3) Based on the quantitative analysis results, a reduced-order model is proposed, which improves the model accuracy without increasing complexity compared with the conventional model reduction methods.

The rest part of this paper is organized as follows. Section II briefly introduces the grid-tied inverter system, and a detailed small-signal model is established. In Section III, a two degrees-of-freedom oscillator model with fast dynamics as excitation is developed. Section IV reveals the impact of the fast dynamics on system stability based on the damping torque analysis. Moreover, a reduced-order model considering the main component of fast dynamics is further proposed. In Section V, numerical evaluations and experiments are conducted to verify the theoretical analysis. Section VI gives concluding remarks.

II. System Description And Modeling

A. System Description

A typical grid-tied inverter with a dual-loop structure [24] is illustrated in Fig. 1. The most commonly used two-level inverter is adopted here, and the analysis process for other topologies is the same. There are three control loops: PLL, dc-link voltage control loop, and current control loop. The power input on the dc side can be wind power, photovoltaic, or other renewable energy power generation devices. $U_{\rm g}$ and $\theta_{\rm g}$ are the magnitude and phase of grid voltage. $U_{\rm t}$ and $\theta_{\rm t}$ are the magnitude and phase of the terminal voltage. θ is the output phase of the PLL. $U_{\rm dc}$ and C are the voltage and capacitance of the dc-side capacitor. $L_{\rm g}$ and $R_{\rm g}$ are the equivalent inductance and resistance of the network; L and R are the inductance and resistance of the ac-side filter. $P_{\rm in}$ and $P_{\rm e}$ are active power input and output. The subscripts

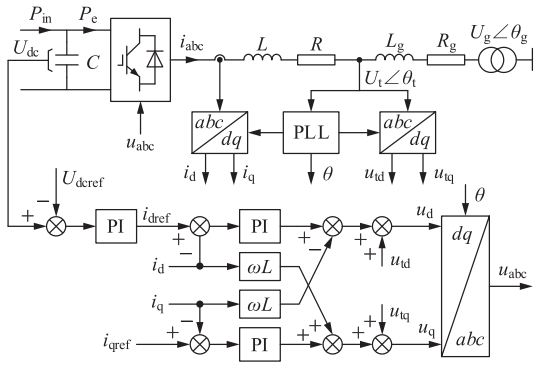

Fig. 1. The diagram of the grid-tied inverter system.

TABLE I
Inverter Parameters for Numerical Evaluations

Symbol	Value	Symbol	Value
$P_{\rm in}$	50 kW	L, R	1 mH, 0.05Ω
$U_{\rm g}$	310 V	$L_{\rm g}$, $R_{\rm g}$	4.3 mH, 0.3Ω
$U_{\rm dc}$	800 V	$k_{\rm vp}$, $k_{\rm vi}$	0.8, 60
$C_{\rm dc}$	4700 μF	$k_{\rm pp}$, $k_{\rm pi}$	0.4, 50
ω_0	314 rad/s	$k_{\rm ip}$, $k_{\rm ii}$	1.8, 150

"d" and "q" indicate the d and q components, "ref" indicates the reference value.

The bandwidths of the controllers are critical to the stability of the inverter. High bandwidths of the dc-link voltage control loop and the PLL is beneficial to quicken the dynamic response; nevertheless, it is not conducive to system stability and even causes the instability phenomenon [26], [27]. Therefore, the choice of bandwidths should be a tradeoff between dynamic response and stability. Reference [28] suggests that the bandwidth of PLL should be lower than the system's fundamental frequency. Also, the bandwidths of the dc-link voltage control loop and the PLL should not be too close; otherwise, the interaction between the controllers will deteriorate the stability [14]. Besides, it is pointed out in [29] that the bandwidth of the current controller should be ten times larger than the outer loop controller. Taking these into consideration, the control parameters and system parameters in this paper are shown in Table I. $k_{\rm vp}$ and $k_{\rm vi}$ are the parameters of the dc-link voltage controller, the bandwidth is about 20 Hz. $k_{\rm pp}$ and $k_{\rm pi}$ are the PLL parameters, the bandwidth is about 30 Hz. $k_{\rm ip}$ and $k_{\rm ii}$ are the current controller parameters, the bandwidth is about 300 Hz.

B. Modeling

In the modeling, the filter and grid resistances are ignored for simplicity since their value are relatively small compared to the reactances. If the resistances are considered, the analysis method and conclusions in this paper are applicable, but it will make the analysis process extremely complicated. The mathematical expressions considering the resistance are also given in Appendix. Here will take the analysis ignoring the resistance as an example.

Authorized licensed use limited to: SICHUAN UNIVERSITY. Downloaded on June 06,2022 at 09:26:40 UTC from IEEE Xplore. Restrictions apply.

Except for grid voltage, the other state variables in the inverter change with the output phase of the PLL. Therefore, it is reasonable to build these state variables under the *d-q* frame with the reference angle of the PLL. It is assumed that the grid voltage is balanced. Then the grid voltage is transformed into the same *d-q* frame as other variables:

$$\begin{cases} u_{\mathrm{gd}} = U_{\mathrm{g}}\cos(\theta_{\mathrm{g}}-\theta) = U_{\mathrm{g}}\cos\varphi \\ u_{\mathrm{gq}} = U_{\mathrm{g}}\sin(\theta_{\mathrm{g}}-\theta) = -U_{\mathrm{g}}\sin\varphi \end{cases} \tag{1}$$

where φ is the phase difference between θ and θ_{g}.

Under the *d-q* frame, the PLL model is expressed as

$$\theta = u_{\mathrm{tq}}\left(k_{\mathrm{pp}} + \frac{k_{\mathrm{pi}}}{s}\right)\frac{1}{s} \tag{2}$$

$$u_{\mathrm{tq}} = \omega L_{\mathrm{g}} i_{\mathrm{d}} + sL_{\mathrm{g}} i_{\mathrm{q}} + u_{\mathrm{gq}} \tag{3}$$

By linearization (2) and (3), the small-signal model of the PLL is derived as

$$\Delta\theta = \Delta u_{\mathrm{tq}}\left(k_{\mathrm{pp}} + \frac{k_{\mathrm{pi}}}{s}\right)\frac{1}{s} \tag{4}$$

$$\Delta u_{\mathrm{tq}} = X_{\mathrm{g}}\Delta i_{\mathrm{d}} + L_{\mathrm{g}} i_{\mathrm{d0}}\Delta\omega + sL_{\mathrm{g}}\Delta i_{\mathrm{q}} - U_{\mathrm{g0}}\cos\varphi_0\Delta\theta \tag{5}$$

where $X_{\mathrm{g}} = \omega_0 L_{\mathrm{g}}$, and the subscripts "0" indicate the value of the variables on the steady operating point.

The dynamics of the dc-link voltage control loop are

$$P_{\mathrm{in}} - P_{\mathrm{e}} = U_{\mathrm{dc}} C\frac{\mathrm{d}U_{\mathrm{dc}}}{\mathrm{d}t} \tag{6}$$

$$i_{\mathrm{dref}} = (U_{\mathrm{dc}} - U_{\mathrm{dcref}})\left(k_{\mathrm{vp}} + \frac{k_{\mathrm{vi}}}{s}\right) \tag{7}$$

$$P_{\mathrm{e}} = \frac{3}{2}(u_{\mathrm{gd}} i_{\mathrm{d}} + u_{\mathrm{gq}} i_{\mathrm{q}}) \tag{8}$$

Under normal operating conditions, the grid-connected VSC is usually controlled with the unity power factor for maximizing the active power output of renewable energy [25], thus there are $i_{\mathrm{q0}} = i_{\mathrm{qref}} = 0$ in steady-state. Linearizing (6)–(8) yields

$$\Delta P_{\mathrm{in}} - \Delta P_{\mathrm{e}} = U_{\mathrm{dc0}} Cs\Delta U_{\mathrm{dc}} \tag{9}$$

$$\Delta i_{\mathrm{dref}} = (\Delta U_{\mathrm{dc}} - \Delta U_{\mathrm{dcref}})\left(k_{\mathrm{vp}} + \frac{k_{\mathrm{vi}}}{s}\right) \tag{10}$$

$$\Delta P_{\mathrm{e}} = \frac{3}{2}(U_{\mathrm{g0}}\cos\varphi_0\Delta i_{\mathrm{d}} - U_{\mathrm{g0}}\sin\varphi_0\Delta i_{\mathrm{q}} - U_{\mathrm{g0}} i_{\mathrm{d0}}\sin\varphi_0\Delta\theta) \tag{11}$$

The dynamics of the current control loop and ac-side filter are represented as

$$(i_{\mathrm{dref}} - i_{\mathrm{d}})\left(k_{\mathrm{ip}} + \frac{k_{\mathrm{ii}}}{s}\right) - \omega_0 L i_{\mathrm{q}} = -\omega L i_{\mathrm{q}} + sL i_{\mathrm{d}} \tag{12}$$

$$(i_{\mathrm{qref}} - i_{\mathrm{q}})\left(k_{\mathrm{ip}} + \frac{k_{\mathrm{ii}}}{s}\right) + \omega_0 L i_{\mathrm{d}} = \omega L i_{\mathrm{d}} + sL i_{\mathrm{q}} \tag{13}$$

By linearization, the small-signal model of (12) and (13) are

$$(\Delta i_{\mathrm{dref}} - \Delta i_{\mathrm{d}})\left(k_{\mathrm{ip}} + \frac{k_{\mathrm{ii}}}{s}\right) = -L i_{\mathrm{q0}}\Delta\omega + sL\Delta i_{\mathrm{d}} \tag{14}$$

$$(\Delta i_{\mathrm{qref}} - \Delta i_{\mathrm{q}})\left(k_{\mathrm{ip}} + \frac{k_{\mathrm{ii}}}{s}\right) = L i_{\mathrm{d0}}\Delta\omega + sL\Delta i_{\mathrm{q}} \tag{15}$$

Assuming $\Delta U_{\mathrm{dcref}} = 0$ and $\Delta i_{\mathrm{qref}} = 0$, according to (4), (5), (9), (10), (14), and (15), the small-signal model of the grid-tied inverter is represented as

$$\Delta i_{\mathrm{dref}} = K_1(\Delta P_{\mathrm{in}} - K_2\Delta i_{\mathrm{d}} - K_5\Delta i_{\mathrm{q}} - K_4\Delta\theta)\left(k_{\mathrm{vp}} + \frac{k_{\mathrm{vi}}}{s}\right)\frac{1}{s} \tag{16}$$

$$\Delta\theta = (X_{\mathrm{g}}\Delta i_{\mathrm{d}} + L_{\mathrm{g}} i_{\mathrm{d0}}\Delta\omega + sL_{\mathrm{g}}\Delta i_{\mathrm{q}} - K_3\Delta\theta)\left(k_{\mathrm{pp}} + \frac{k_{\mathrm{pi}}}{s}\right)\frac{1}{s} \tag{17}$$

$$\Delta i_{\mathrm{d}} = (\Delta i_{\mathrm{dref}} - \Delta i_{\mathrm{d}})(k_{\mathrm{ip}} + \frac{k_{\mathrm{ii}}}{s})\frac{1}{sL} \tag{18}$$

$$\Delta i_{\mathrm{q}} = -\Delta i_{\mathrm{q}}(k_{\mathrm{ip}} + \frac{k_{\mathrm{ii}}}{s})\frac{1}{sL} - i_{\mathrm{d0}}\Delta\theta \tag{19}$$

The parameters K_1 to K_5 are dependent on the steady operating point, and their mathematical expressions are shown in Appendix.

Equation (16) shows the dynamic of the dc-link voltage controller, which is affected by the output current dynamic. Equation (17) is the dynamic equation of the PLL, and its dynamic is affected by the current controller and the network inductance. The dynamics of the current controller and filter inductance are represented by (18) and (19), and they are affected by the dc-link voltage control and PLL. In short, there are complicated coupling between fast dynamics and slow dynamics, and the stability of the system is determined by the interaction between the multi-timescale dynamics.

III. Two Degrees-of-Freedom Oscillator Model

In this section, the conventional reduced-order model that ignores fast dynamics will be presented and expressed in the form of a two degrees-of-freedom oscillator model. Then, the dynamic response of the reduced-order model will be compared with those of the small-signal model, which shows that the neglected fast dynamics also have a certain degree of impact on system stability. Then an oscillator model considering fast dynamics will be developed, in which the fast dynamics are extracted as the excitation of the slow dynamics.

A. Conventional Oscillator Model

Due to the bandwidths of fast dynamics such as current loop and network dynamics is much higher than that of slow dynamics, the conventional model reduction method believes that the output current can catch up with current reference immediately, that is, $\Delta i_{\mathrm{dref}} = \Delta i_{\mathrm{d}}$ and $\Delta i_{\mathrm{qref}} = \Delta i_{\mathrm{q}} = 0$. Therefore, the differential equations (14) and (15) which express current control loop and network dynamics can be transformed

Authorized licensed use limited to: SICHUAN UNIVERSITY. Downloaded on June 06,2022 at 09:26:40 UTC from IEEE Xplore. Restrictions apply.

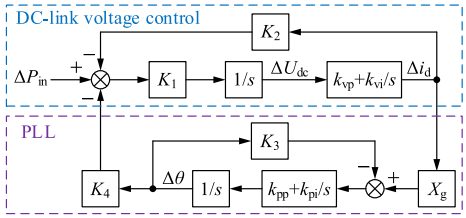

Fig. 2. Block diagram of the conventional reduced-order model.

into an algebraic equation as follows

$$\begin{cases} s\Delta i_{\mathrm{d}} = i_{\mathrm{q0}}\Delta\omega \\ s\Delta i_{\mathrm{q}} = -i_{\mathrm{d0}}\Delta\omega = 0 \end{cases} \tag{20}$$

Substituting (20) into (16) and (17), there is

$$\begin{cases} \Delta i_{\mathrm{d}} = K_1(\Delta P_{\mathrm{in}} - K_2\Delta i_{\mathrm{d}} - K_4\Delta\theta)(k_{\mathrm{vp}} + \frac{k_{\mathrm{vi}}}{s})\frac{1}{s} \\ \Delta\theta = (X_{\mathrm{g}}\Delta i_{\mathrm{d}} - K_3\Delta\theta)(k_{\mathrm{pp}} + \frac{k_{\mathrm{pi}}}{s})\frac{1}{s} \end{cases} \tag{21}$$

Equation (21) is the conventional reduced-order model that ignores fast dynamics and can be depicted in Fig. 2.

The reduced-order model in Fig. 2 only includes the dc-link voltage control loop and PLL, and the two controllers interact with each other. In order to analyze the inverter stability from the physical point of view, the reduced-order model was analogized to two coupled oscillators in [14]. And the corresponding force-free equation can be characterized as

$$\underbrace{\begin{bmatrix} 1 & 0 \\ 0 & 1 \end{bmatrix}}_{\mathbf{M}} \begin{bmatrix} s^2\Delta i_{\mathrm{d}} \\ s^2\Delta\theta \end{bmatrix} + \underbrace{\begin{bmatrix} d_{11} & d_{12} \\ d_{21} & d_{22} \end{bmatrix}}_{\mathbf{D}} \begin{bmatrix} s\Delta i_{\mathrm{d}} \\ s\Delta\theta \end{bmatrix} + \underbrace{\begin{bmatrix} k_{11} & k_{12} \\ k_{21} & k_{22} \end{bmatrix}}_{\mathbf{K}} \begin{bmatrix} \Delta i_{\mathrm{d}} \\ \Delta\theta \end{bmatrix} = 0 \tag{22}$$

In which $\boldsymbol{M}$, $\boldsymbol{D}$, and $\boldsymbol{K}$ represent the mass, damping, and spring coefficients matrices, respectively. The diagonal elements d_{ii} and k_{ii} $(i = 1, 2)$ are related to the respective oscillation modes of the dc-link voltage control loop and the PLL, while the off-diagonal elements d_{ij} and k_{ij} $(j = 1, 2, i \neq j)$ denote the interaction between the two controllers. According to (21), the coefficient matrix $\boldsymbol{D}$ and $\boldsymbol{K}$ are obtained as follows

$$\mathbf{D} = \begin{bmatrix} K_1K_2k_{\mathrm{vp}} & K_1K_4k_{\mathrm{vp}} \\ -X_{\mathrm{g}}k_{\mathrm{pp}} & K_3k_{\mathrm{pp}} \end{bmatrix} \mathbf{K} = \begin{bmatrix} K_1K_2k_{\mathrm{vi}} & K_1K_4k_{\mathrm{vi}} \\ -X_{\mathrm{g}}k_{\mathrm{pi}} & K_3k_{\mathrm{pi}} \end{bmatrix} \tag{23}$$

The small-signal model in (16)-(19) is an eighth-order equation, and the reduced-order model represented by (22) is a fourth-order equation. Ignoring fast dynamics does greatly reduce the complexity of the system, but it will inevitably lead to errors in modeling.

In order to intuitively show the model error induced by fast dynamics, the dynamic response of the detailed model, the small-signal model, and the reduced-order model are compared with each other. The detailed model is built in MATLAB/Simulink, a constant power source is used on the dc side to represent the power input, and a power disturbance of 0.2% is applied in 0.2s. In order to eliminate the influence of switching sub-harmonics,

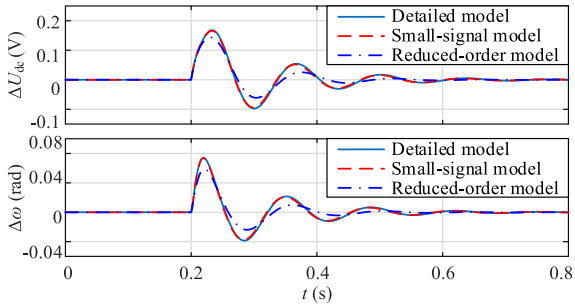

Fig. 3. Comparison of dynamic response among detailed model, small-signal model, and conventional reduced-order model.

an average model of the inverter is used [14]. The small-signal model and the reduced-order model are programmed in MATLAB to realize time-domain simulation. Fig. 3 shows the comparisons of the dc-link voltage and phase dynamics among the three models. It is observed that the dynamic of the small-signal model is in good accord with the detailed model, while there are obvious differences in the dynamic response of the reduced-order and the detailed model. This implies that ignoring the fast dynamics will cause an unacceptable deviation in model accuracy, which will bring misjudgment on stability analysis.

B. The Proposed Oscillator Model

In order to analyze the impact of fast dynamics, this part proposes a model similar to (22), which extracts fast dynamics separately from the small-signal model.

Equations (18) and (19) can be reorganized as follow

$$\begin{cases} \Delta i_{\mathrm{d}} = \frac{k_{\mathrm{ip}}s + k_{\mathrm{ii}}}{Ls^2 + k_{\mathrm{ip}}s + k_{\mathrm{ii}}}\Delta i_{\mathrm{dref}} \\ \Delta i_{\mathrm{q}} = -\frac{i_{\mathrm{d0}}Ls^2}{Ls^2 + k_{\mathrm{ip}}s + k_{\mathrm{ii}}}\Delta\theta \end{cases} \tag{24}$$

Define

$$A(s) = \frac{k_{\mathrm{ip}}s + k_{\mathrm{ii}}}{Ls^2 + k_{\mathrm{ip}}s + k_{\mathrm{ii}}} \tag{25}$$

Considering $K_4 = K_5 i_{\mathrm{d0}}$, then substituting (24) and (25) into (16) and (17), the small-signal model can be transformed as

$$\begin{cases} \Delta i_{\mathrm{d}} = K_1A(s)\left[\Delta P_{\mathrm{in}} - K_2\Delta i_{\mathrm{d}} - K_4A(s)\Delta\theta\right](k_{\mathrm{vp}} + \frac{k_{\mathrm{vi}}}{s})\frac{1}{s} \\ \Delta\theta = \left[X_{\mathrm{g}}\Delta i_{\mathrm{d}} + L_{\mathrm{g}}i_{\mathrm{d0}}sA(s)\Delta\theta - K_3\Delta\theta\right](k_{\mathrm{pp}} + \frac{k_{\mathrm{pi}}}{s})\frac{1}{s} \end{cases} \tag{26}$$

Equation (26) represents the small-signal model in a form similar to (21). The corresponding block diagram is shown in Fig. 4. The red parts are the additional items introduced by the fast dynamics compared with Fig. 2. $A(s)$ is the closed-loop transfer function of the current control loop as shown in (25), the dynamics of the current controller and filter inductor are incorporated in it. The differential term of $L_{\mathrm{g}}i_{\mathrm{d0}}s$ represents the dynamic of the network inductance.

Further reorganize (26), place the slow dynamics of the dc-link voltage control loop and PLL on the left side of the equal sign, the fast dynamics represented by the red part in Fig. 4 are

Authorized licensed use limited to: SICHUAN UNIVERSITY. Downloaded on June 06,2022 at 09:26:40 UTC from IEEE Xplore. Restrictions apply.

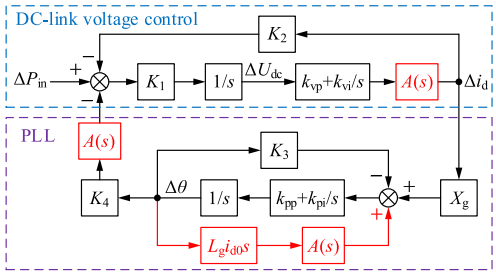

Fig. 4. Block diagram of the small-signal model.

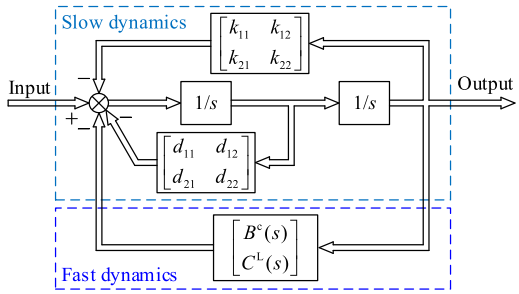

Fig. 5. Schematic diagram of equation (31).

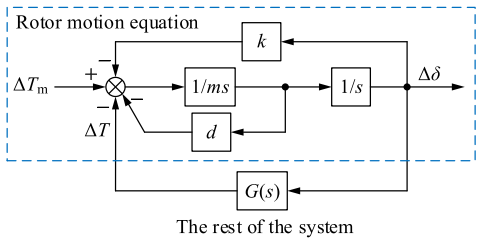

Fig. 6. Diagram of damping torque analysis for single-machine infinite-bus system.

extracted and placed on the right side, it can obtain.

$$s^2\Delta i_{\rm d} - K_1(\Delta P_{\rm in} - K_2\Delta i_{\rm d} - K_4\Delta\theta)(k_{\rm vp}s + k_{\rm vi}) = -\frac{Ls^4}{k_{\rm ip}s + k_{\rm ii}}\Delta i_{\rm d} + \frac{K_1K_4Ls^2(k_{\rm vp}s + k_{\rm vi})}{Ls^2 + k_{\rm ip}s + k_{\rm ii}}\Delta\theta \quad (27)$$

$$s^2\Delta\theta - (X_{\rm g}\Delta i_{\rm d} - K_3\Delta\theta)(k_{\rm vp}s + k_{\rm vi}) = L_{\rm g}i_{\rm d0}s(k_{\rm pp}s + k_{\rm pi})A(s)\Delta\theta \quad (28)$$

Because the eigenvalues of the system are not related to the input, there is a quantitative conversion relationship between $\Delta i_{\rm d}$ and $\Delta\theta$ when the input is ignored according to the first equation of (26). The corresponding relationship is as follow

$$\Delta\theta = -\frac{s^2}{K_1K_4A(s)^2(k_{\rm vp}s + k_{\rm vi})}\Delta i_{\rm d} - \frac{K_2}{K_4A(s)}\Delta i_{\rm d} \quad (29)$$

Applying the conversion relationship in (29) to the right side of (27), it can obtain.

$$s^2\Delta i_{\rm d} - K_1(\Delta P_{\rm in} - K_2\Delta i_{\rm d} - K_4\Delta\theta)(k_{\rm vp}s + k_{\rm vi}) = -\frac{K_1K_2Ls^2(k_{\rm vp}s + k_{\rm vi})}{k_{\rm ip}s + k_{\rm ii}}\Delta i_{\rm d} - \frac{Ls^4\left[1 + A(s)\right]}{(k_{\rm ip}s + k_{\rm ii})A(s)}\Delta i_{\rm d} \quad (30)$$

The bandwidth of the current control loop is usually designed to be much larger than the slow dynamics, so it can be considered that $A(s) \approx 1$ in (28) and (30) holds when the stability dominated by the slow dynamics is focused. This simplification will not bring obvious errors in the accuracy of the model, which will be verified in the comparison of the eigenvalues later; but it can greatly reduce the complexity of the impact analysis of fast dynamic. Analogize to (22), a two degrees-of-freedom oscillator model can be extended as (31) by combining (28) and (30), in which the fast dynamics are extracted to the right side and regarded as excitations of the slow dynamics.

$$\begin{bmatrix}1&0\\0&1\end{bmatrix}\begin{bmatrix}s^2\Delta i_{\rm d}\\ s^2\Delta\theta\end{bmatrix} + \begin{bmatrix}d_{11}&d_{12}\\d_{21}&d_{22}\end{bmatrix}\begin{bmatrix}s\Delta i_{\rm d}\\ s\Delta\theta\end{bmatrix} + \begin{bmatrix}k_{11}&k_{12}\\k_{21}&k_{22}\end{bmatrix}\begin{bmatrix}\Delta i_{\rm d}\\ \Delta\theta\end{bmatrix} = \begin{bmatrix}-B^{\rm c}(s)\\-C^{\rm L}(s)\end{bmatrix}\begin{bmatrix}\Delta i_{\rm d}\\ \Delta\theta\end{bmatrix} \quad (31)$$

The proposed oscillator model can be depicted by the schematic diagram in Fig. 5. And the mathematical expressions of $B^{\rm c}(s)$ and $C^{\rm L}(s)$ are shown in Appendix. It is worth noting that the fast dynamics in (31) realize decoupling through the transformation and simplification of the equations. $B^{\rm c}(s)$ represents the dynamic of the current control loop, which mainly affects the dc-link voltage control loop, and $C^{\rm L}(s)$ describes the dynamic of the network inductance, which mainly affects the dynamic of PLL. This decoupling is conducive to further analysis.

In this way, the fast dynamics have been extracted separately, so the impact of the fast dynamic on the system stability can be quantified by analyzing the influence of $B^{\rm c}(s)$ and $C^{\rm L}(s)$ on the damping and spring coefficients of the system.

IV. Impact Analysis of Fast Dynamics

In order to get a quantitative understanding, the damping torque analysis will be applied in this section to analyze the extracted fast dynamics in the proposed oscillator model. The fast dynamics will be decomposed into additional damping and spring coefficients. The variation of the additional coefficients with the parameters will be explored. Moreover, based on the quantitative analysis, a novel reduced-order model is further proposed.

A. Damping Torque Analysis

The damping torque analysis originated from the analysis of the linearized model of a single-machine infinite-bus system, which was used to evaluate the influence of excitation control on synchronous machine stability [30]. Its physical essence is to reduce the order of the original system under the condition of retaining the dominant eigenvalues.

The diagram of the damping torque analysis for the single-machine infinite-bus system is shown in Fig. 6. The system is divided into a rotor motion equation and the corresponding remainder composed of excitation control and external system which are described by $G(s)$. The remainder provides additional electromagnetic torque ΔT for the rotor motion equation. If the disturbance of mechanical torque $\Delta T_{\rm m}$ is ignored, the equation

Authorized licensed use limited to: SICHUAN UNIVERSITY. Downloaded on June 06,2022 at 09:26:40 UTC from IEEE Xplore. Restrictions apply.

of a single-machine infinite-bus system can be written as

$$ms^2\Delta\delta + ds\Delta\delta + k\Delta\delta = -\Delta T \tag{32}$$

The left side of (32) is the rotor motion equation, and the ΔT on the right side can be regarded as the excitation of the left side. Assuming that the dominant eigenvalues of the system are $s = \sigma + \mathrm{j}\omega_\mathrm{n}$, the damping torque analysis is to decompose ΔT into

$$\begin{aligned}\Delta T &= G(s)\Delta\delta \approx G(\sigma+\mathrm{j}\omega_\mathrm{n})\Delta\delta \\ &= \left(\mathrm{Re}\left[G(\sigma+\mathrm{j}\omega_\mathrm{n})\right] + \mathrm{jIm}\left[G(\sigma+\mathrm{j}\omega_\mathrm{n})\right]\right)\Delta\delta \\ &= k_\mathrm{T}\Delta\delta + d_\mathrm{T}(\sigma+\mathrm{j}\omega_\mathrm{n})\Delta\delta \\ &\approx k_\mathrm{T}\Delta\delta + d_\mathrm{T}s\Delta\delta \end{aligned} \tag{33}$$

In which

$$\begin{aligned} d_\mathrm{T} &= \tfrac{1}{\omega_\mathrm{n}}\mathrm{Im}\left[G(\sigma+\mathrm{j}\omega_\mathrm{n})\right] \\ k_\mathrm{T} &= \mathrm{Re}\left[G(\sigma+\mathrm{j}\omega_\mathrm{n})\right] - \tfrac{\sigma}{\omega_\mathrm{n}}\mathrm{Im}\left[G(\sigma+\mathrm{j}\omega_\mathrm{n})\right] \end{aligned} \tag{34}$$

According to (33) and (34), the influence of the remainder on the rotor motion equation is decomposed into damping and synchronization coefficient while approximately preserving the dynamics of the remainder around dominant eigenvalues.

Substituting (33) into (32), there is

$$ms^2\Delta\delta + (d+d_\mathrm{T})s\Delta\delta + (k+k_\mathrm{T})\Delta\delta = 0 \tag{35}$$

The total damping and synchronization coefficients of the single-machine infinite-bus system change from d and k to $d+d_\mathrm{T}$ and $k+k_\mathrm{T}$, respectively. In this way, the effect of the remainder on system stability can be quantified by d_T and k_T.

For the oscillator model of the grid-tied inverter, the comparison between Fig. 5 and Fig. 6 shows that the proposed model expressed in (31) and the single-machine infinite-bus model are the same in form but different in model order. Thus, the damping torque analysis can be applied to quantify the impact of fast dynamics on inverter stability. Then the transfer function of fast dynamics in (31) can be decomposed by substituting $s = \sigma + \mathrm{j}\omega_\mathrm{n}$ as follow

$$\begin{cases} B^\mathrm{c}(s)\Delta i_\mathrm{d} \approx B^\mathrm{c}(\sigma+\mathrm{j}\omega_\mathrm{n})\Delta i_\mathrm{d} \approx d_{11}^\mathrm{c}s\Delta i_\mathrm{d} + k_{11}^\mathrm{c}\Delta i_\mathrm{d} \\ C^\mathrm{L}(s)\Delta\theta \approx D^\mathrm{L}(\sigma+\mathrm{j}\omega_\mathrm{n})\Delta i_\mathrm{d} \approx d_{22}^\mathrm{L}s\Delta\theta + k_{22}^\mathrm{L}\Delta\theta \end{cases} \tag{36}$$

In which the expressions of the coefficients are shown in Appendix.

Substituting (36) into (31), the damping torque model of the inverter expressed by (37) can be obtained. In which, d_{11}^c and k_{11}^c affect the dynamic of the dc-link voltage control loop, their values are related to the parameters of the current controller and dc-link voltage controller; d_{22}^L and k_{22}^L affect the dynamic of PLL, which values are determined by the parameters of network inductance and PLL. So far, fast dynamics have been quantified as the impact on damping and spring coefficients of slow dynamic.

$$\begin{bmatrix}1 & 0\\ 0 & 1\end{bmatrix}\begin{bmatrix}s^2\Delta i_\mathrm{d}\\ s^2\Delta\theta\end{bmatrix} + \begin{bmatrix}d_{11}+d_{11}^\mathrm{c} & d_{12}\\ d_{21} & d_{22}+d_{22}^\mathrm{L}\end{bmatrix}\begin{bmatrix}s\Delta i_\mathrm{d}\\ s\Delta\theta\end{bmatrix} + \begin{bmatrix}k_{11}+k_{11}^\mathrm{c} & k_{12}\\ k_{21} & k_{22}+k_{22}^\mathrm{L}\end{bmatrix}\begin{bmatrix}\Delta i_\mathrm{d}\\ \Delta\theta\end{bmatrix} = 0 \tag{37}$$

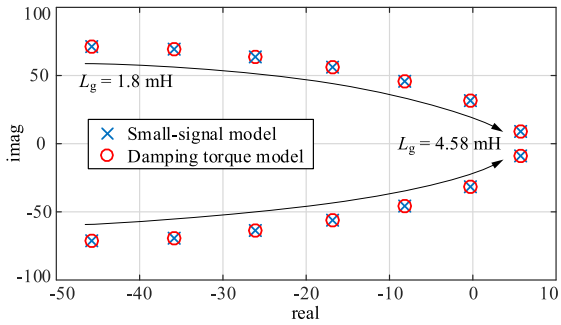

Fig. 7. Dominant eigenvalues locus of the small-signal model and the damping torque model with L_g varies from 1.8 mH to 4.58 mH.

To verify the effectiveness of the damping torque analysis, the eigenvalues comparison between the small-signal model with the damping torque model expressed by (37) is conducted. The eigenvalues of the damping torque model can be obtained by solving the characteristic equation of (37). To obtain the eigenvalues of the small-signal model, it is necessary to convert (16)-(19) into the form of state-space equations and find the eigenvalues of the state matrix. Since the establishment of the state space equations has been introduced in many pieces of literature, it will not be repeated in this paper for the sake of simplicity. As the dynamic of the grid-tied inverter is determined by dominant eigenvalues, Fig. 7 shows the dominant eigenvalues locus of the damping torque model and the small-signal model with L_g varies from 1.8 mH to 4.58 mH. It is observed that the eigenvalues of the two models almost coincide, indicating that the damping torque model is accurate.

B. Quantitative Analysis of Fast Dynamics on Stability

The impact of fast dynamics on the system stability can be obtained by analyzing the variation of the additional coefficients with the parameters. The fast dynamics can be subdivided into the dynamics of the current control loop and the network inductance. Thus, the fast dynamics parameters can be covered by the bandwidth of the current control loop and the value of the inductance. To intuitively show the influence of the additional coefficient, the ratio of the additional coefficient to the corresponding coefficient of slow dynamics is given in the form of graphs. A positive ratio indicates a positive impact, and a negative ratio indicates a negative impact.

1) Impact of Current Control Loop Bandwidth: Fig. 8 shows the variation of the additional coefficients with the bandwidth of the current control loop. It can be observed that with the decrease of bandwidth, the ratio of additional coefficients d_{22}^L/d_{22} and k_{22}^L/k_{22} is almost unchanged, while the absolute values of d_{11}^c/d_{11} and k_{11}^c/k_{11} increase slightly. In addition, when the bandwidth of the current control loop approaches to that of the dc-link voltage control loop and PLL, the change of d_{11}^c/d_{11} and k_{11}^c/k_{11} is more obvious, which reflects that the interaction between the current controller and the slow dynamic becomes stronger as the bandwidths approach. Nonetheless, the bandwidth of the current control loop is usually much higher than that of the dc-link voltage control loop and PLL [29], that

Authorized licensed use limited to: SICHUAN UNIVERSITY. Downloaded on June 06,2022 at 09:26:40 UTC from IEEE Xplore. Restrictions apply.

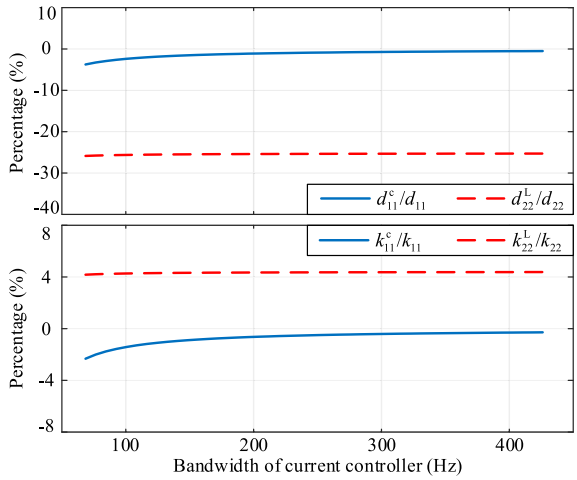

Fig. 8. The additional coefficients vary with the bandwidth of the current control loop.

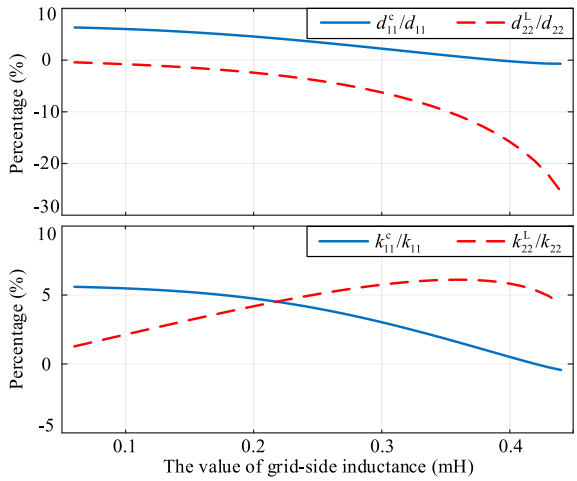

Fig. 9. The additional coefficients vary with the network inductance.

is, the bandwidth of the current controller is hundreds of Hz. In this case, the bandwidth change only has a slight effect on the additional coefficients, so the effect of the bandwidth variation can be ignored.

2) Impact of Network Inductance: Fig. 9 shows the variation of the additional coefficients with the value of network inductance. The additional coefficients change greatly with the variation of the inductance. Since the stability of the system is mainly determined by the damping of the eigenvalues, the variation characteristics of the damping coefficients should be paid attention to first.

With the increase of the network inductance, the absolute value of $d_{22}^{\mathrm{L}}/d_{22}$ increases rapidly, and its value is always less than zero. That is to say, the dynamic of the network inductance always reduces the system damping, especially when the value of the inductance is large. In addition, since the value of d_{22}^{L} will decrease as the control parameters of the PLL increase according to its mathematical expression, the larger the proportional and integral coefficients are, the more damping degradation will be caused by the inductance dynamics. In other words, larger control parameters may not increase the response speed of PLL but worsen the system stability. Besides, the value of d_{22}^{L} is related to the damping of the dominant eigenvalues, the impact of inductance dynamic on system stability will get larger as the dominant eigenvalues approaching the imaginary axis.

On the other hand, $d_{11}^{\mathrm{c}}/d_{11}$ is greater than zero when the network inductance is small, and its value will gradually decrease to less than zero as the inductance increases. That is to say, when the network inductance is small, the dynamics of the current control loop is conducive to system stability. Additionally, the mathematical expression of d_{11}^{c} does not contain the network inductance, but it is affected by the dominant eigenvalues. The increase of the inductance leads to the dominant eigenvalues approach to the imaginary axis, which decreases the value of d_{11}^{c}. In other words, the closer the dominant eigenvalue is to the imaginary axis, the less influence the current control loop on the system stability, which is just opposite to that of the inductance dynamic.

For the additional spring constant introduced by fast dynamics, its value is greater than zero under most inductance conditions, that is, fast dynamics will increase the frequency of system oscillation. However, due to the value of $k_{11}^{\mathrm{c}}/k_{11}$ and $k_{22}^{\mathrm{L}}/k_{22}$ in Fig. 9 is small and the square relationship between the oscillation frequency and the spring coefficient, the additional spring coefficients have little effect on the oscillation frequency of the dominant eigenvalue.

C. Application for Model Reduction

The purpose of model reduction is to reduce the complexity of the system while retaining the original system dynamics so as to reveal the internal mechanism of system instability intuitively. This part will present the application of the quantitative analysis above for model reduction, and an accurate reduced order model will be proposed in the following.

In the proposed two degrees-of-freedom oscillator model expressed by (31), the fast dynamics are decoupled into the current control loop dynamic and the network inductance dynamic. The analysis results show that when the dominant eigenvalues approach the imaginary axis, the inductance dynamic has a great impact on the system stability, while the effect of the current control loop dynamics is small. When analyzing the mechanism of system instability or investigating the boundary of the parameters, we usually pay more attention to the cases of the dominant eigenvalue approach to the imaginary axis, that is, when the system will be unstable. In this case, the current dynamic control loop can be ignored due to its small influence, while the network inductance dynamic needs to be retained. Thus, it can be considered that the transfer function representing the contribution of the current control loop dynamic in (31) is equal to zero, that is, $B^{\mathrm{c}}(s)=0$. Then (31) can be transformed into the same form as (21) expressed by the conventional reduced-order model, and the proposed reduced-order model in this paper is derived as follows

$$\begin{cases} \Delta i_{\mathrm{d}} = K_1\left[\Delta P_{\mathrm{in}} - K_2\Delta i_{\mathrm{d}} - K_4\Delta\theta\right]\left(k_{\mathrm{vp}} + \frac{k_{\mathrm{vi}}}{s}\right)\frac{1}{s} \\ \Delta\theta = \left[X_{\mathrm{g}}\Delta i_{\mathrm{d}} + L_{\mathrm{g}} i_{\mathrm{d0}} s\Delta\theta - K_3\Delta\theta\right]\left(k_{\mathrm{pp}} + \frac{k_{\mathrm{pi}}}{s}\right)\frac{1}{s} \end{cases} \tag{38}$$

Authorized licensed use limited to: SICHUAN UNIVERSITY. Downloaded on June 06,2022 at 09:26:40 UTC from IEEE Xplore. Restrictions apply.

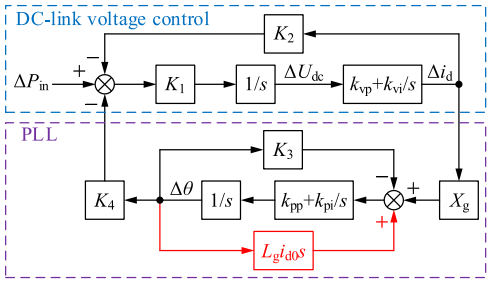

Fig. 10. Block diagram of the proposed reduced-order model.

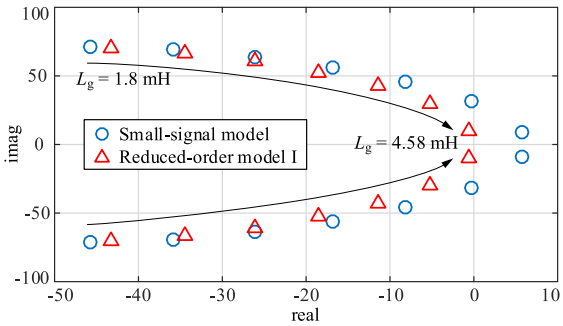

Fig. 11. Dominant eigenvalues locus of the conventional reduced-order model and the small-signal model with L_g varies from 1.8 mH to 4.58 mH.

The proposed reduced-order model can be represented by the block diagram of Fig. 10. Compared with the conventional reduced-order model in Fig. 2, a differential feedforward term is added to indicate the dynamics of the network inductance, which is represented by red color in Fig. 10. The additional term does not increase the order of the reduced-order model but only changed the coefficients of the state space model expression. It is implied that the complexity of the conventional reduced-order model is the same as that of the proposed reduced-order model. The comparative verification of the proposed reduced-order model will be conducted in Section V.

V. Validation

This section will present numerical evaluations and experiments for validation. For the convenience of marking in the figure, the conventional reduced-order model will be called reduced-order I and the proposed reduced-order model in this paper will be called reduced-order model II.

A. Numerical Evaluations

1) Verification of the Impact of Fast Dynamics on Stability: Fig. 11 shows the dominant eigenvalues locus of the conventional reduced-order model and the small-signal model with L_g varies from 1.8 mH to 4.58 mH. The diversity of eigenvalues between the two models in Fig. 11 is induced by the fast dynamics. It is observed that as L_g increases, the eigenvalues of the small-signal model gradually change from the left side to the right side compared to the eigenvalues of the reduced-order model I, and the eigenvalues deviation of the two models get bigger with the increase of L_g. Besides, when L_g is further increased,

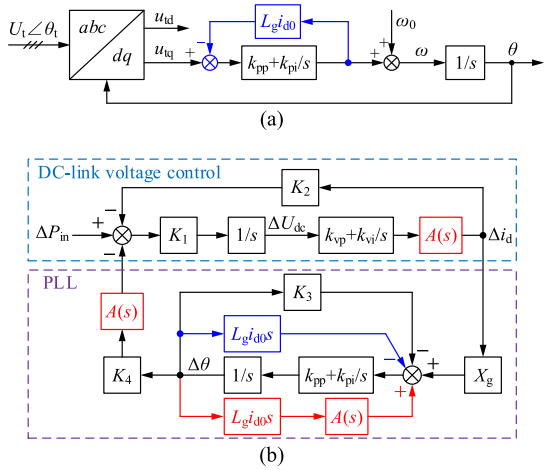

Fig. 12. The negative feedback control scheme. (a) The negative feedback control scheme in PLL. (b) The corresponding small-signal model.

the eigenvalues of the small-signal model have entered the right half-plane, but the reduced-order model I is still stable. These indicate that fast dynamics have a certain degree of influence on system stability, which cannot be ignored, and the influence is not monotonous.

According to the analysis in Section IV, when L_g is small, the current control loop has a greater impact on the system dynamics, and the dynamics of the current control loop can increase the damping of the inverter; so the eigenvalues of the small-signal model are on the left side of those of the reduced-order model I. As the value of inductance increases, the impact of the current control loop decreases, while the influence of the inductance increases rapidly. The dynamics of the network inductance will reduce the system damping, so the eigenvalues of the small-signal model are on the right side of those of the reduced-order model I when L_g is large. Additionally, owing to the fast dynamics will increase the oscillation frequency of slow dynamics, the frequency of the eigenvalues of the small-signal model is slightly larger than that of the reduced-order model I. In summary, the quantitative analysis of fast dynamics in Section IV. B can exactly explain the phenomenon of Fig. 11.

Moreover, hardware-in-the-loop simulations are carried out for verification. The grid-connected VSC together with the weak grid are implemented in a real-time simulator (OPAL-RT OP5607). A constant power source is used on the dc-side of the VSC to simulate the maximum power point tracking of renewable energy. The control algorithms were executed on a DSP controller (TMS320F28335). The time step of the real-time simulator is 5μs. The sampling frequency and the frequency of PWM are both 10 kHz. The network inductance in simulations is 4.1mH, and other parameters are shown in Table I.

The impact of the current control loop on stability can be tested easily by changing the current controller parameters, while the impact of the network inductance dynamic cannot be directly verified by simulations. Considering that the dynamic of the network inductance is equivalent to introducing a positive feedback loop into PLL as shown in Fig. 4, thus a negative feedback loop can be added to the PLL algorithm in simulations

Authorized licensed use limited to: SICHUAN UNIVERSITY. Downloaded on June 06,2022 at 09:26:40 UTC from IEEE Xplore. Restrictions apply.

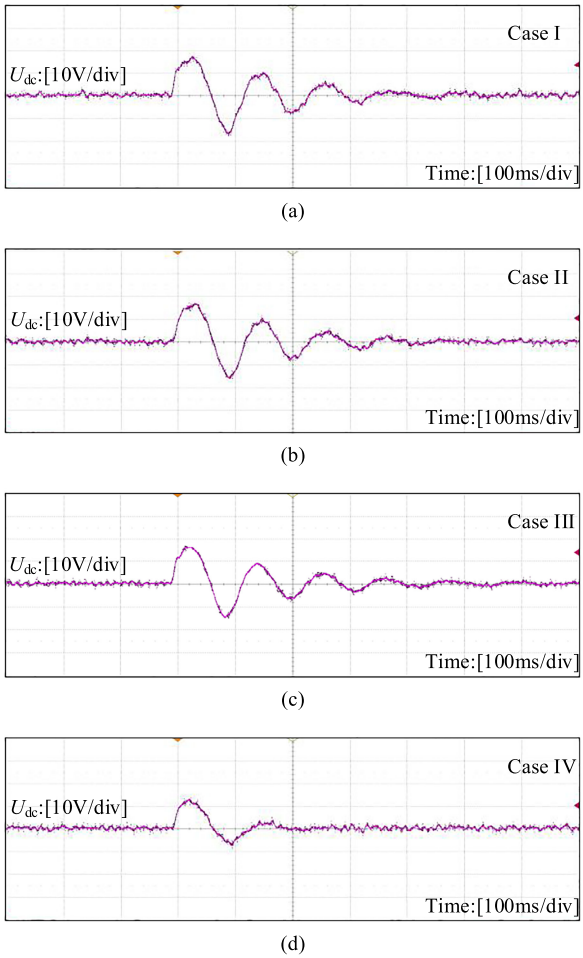

Fig. 13. Hardware-in-the-loop simulation results with four designed cases. (a) Case I. (b) Case II. (c) Case III. (d) Case IV.

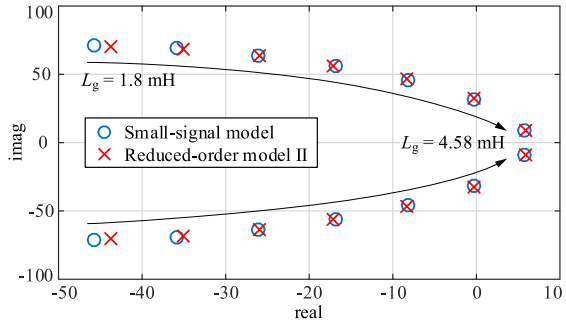

Fig. 14. Dominant eigenvalues locus of the proposed reduced-order model and the small-signal model with L_g varies from 1.8 mH to 4.58 mH.

to indirectly verify the impact of the positive feedback loop. The corresponding control scheme is shown in the blue parts of Fig. 12(a); (b) is the block diagram of the small-signal model considering negative feedback control. And four different cases are designed for verification, which are summarized as follow:

Case I: $k_{ip} = 1.8$, $k_{ii} = 150$, bandwidth = 300 Hz;
Case II: $k_{ip} = 3$, $k_{ii} = 500$, bandwidth = 500 Hz;
Case III: $k_{ip} = 6$, $k_{ii} = 2000$, bandwidth = 1000 Hz;
Case IV: $k_{ip} = 1.8$, $k_{ii} = 150$, bandwidth = 300 Hz, with negative feedback control scheme.

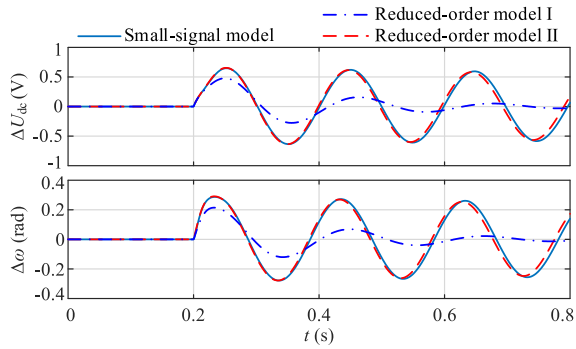

Fig. 15. Comparison of dynamic response among small-signal model, conventional reduced-order model, and proposed reduced-order model when L_g = 4.45 mH.

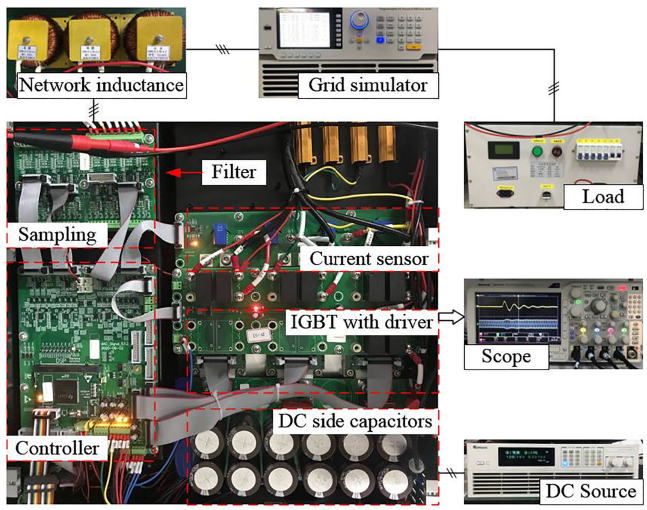

Fig. 16. Configuration of the experimental setup.

Fig. 13 shows the simulation results. The fluctuation of dc-side voltage is induced by a power disturbance of 0.05p.u.. The comparison among (a), (b), and (c) of Fig. 13 shows that the responses of the inverter are basically the same under different current controller parameters. This means that the current control loop has a slight effect on the inverter dynamics, that is, the dynamic of the current control loop has a slight effect on the inverter stability. Besides, the comparison between (a) and (d) of Fig. 13 shows that the negative feedback loop can speed up the response of the inverter, that is, increase the system damping. It indicates that as opposed to the negative feedback loop, the positive feedback loop introduced by the network inductance will decrease the system damping instead, which will deteriorate stability. The above simulation results verify the analysis of Section IV. B.

2) Accuracy of the Proposed Reduced-Order Model: In order to verify the accuracy of the proposed reduced-order model, the dominant eigenvalues locus of the proposed reduced-order model and the small-signal model are implemented as shown in Fig. 14. As can be seen, due to the consideration of the dynamics of the network inductance, the eigenvalues of the proposed reduced-order model are consistent with those of the

Authorized licensed use limited to: SICHUAN UNIVERSITY. Downloaded on June 06,2022 at 09:26:40 UTC from IEEE Xplore. Restrictions apply.

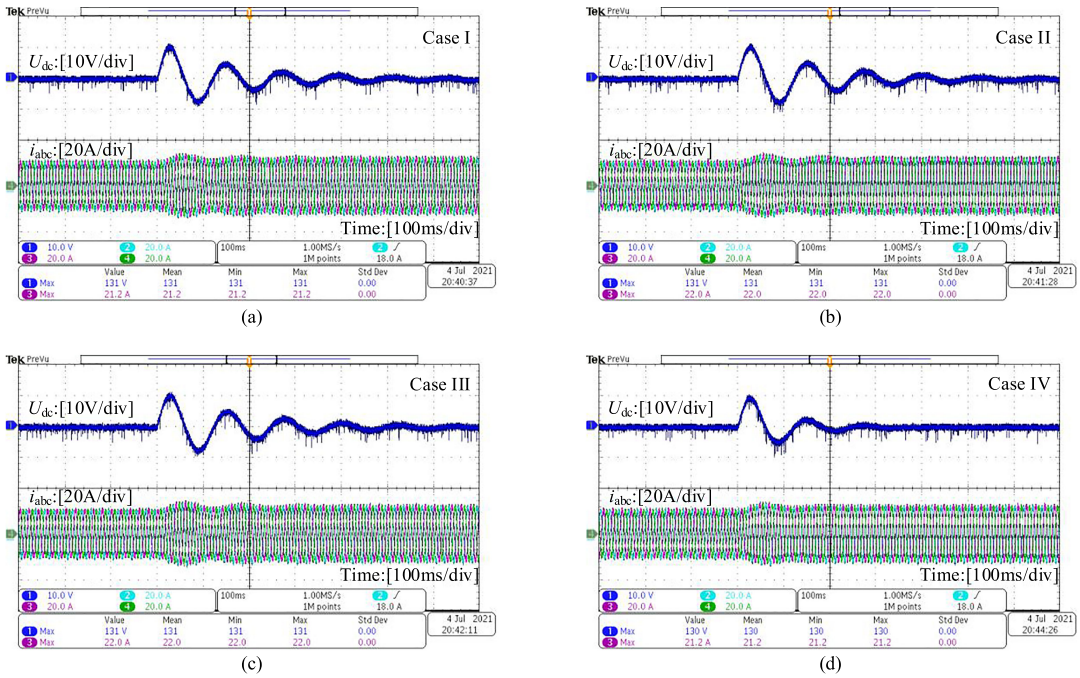

Fig. 17. Experimental results of the grid-connected inverter with different bandwidth of current control loop under grid voltage disturbance. (a) Case I: bandwidth = 300 Hz. (b) Case II: bandwidth = 500 Hz. (c) Case III: bandwidth = 1000 Hz. (d) Case IV: bandwidth = 300 Hz, with negative feedback control scheme.

TABLE II
INVERTER PARAMETERS FOR EXPERIMENTS

Symbol	Value	Symbol	Value
P_{in}	1kW	L	1 mH
U_g	45V	L_g	4.5 mH
U_{dc}	120V	k_{vp}, k_{vi}	0.05, 10
C_{dc}	1645 μF	k_{pp}, k_{pi}	2.5, 320
ω_0	314 rad/s	k_{ip}, k_{ii}	1.8, 150

small-signal model, especially when the eigenvalues approach the imaginary axis. Compared with the eigenvalues of the conventional reduced-order model in Fig. 11, the proposed reduced-order model greatly improves the accuracy of order reduction.

Fig. 15 shows the comparison of dynamic responses among the small-signal model, the conventional reduced-order model, and the proposed reduced-order model. For the convenience of marking in the figure, the conventional reduced-order model is called reduced-order I and the proposed reduced-order model is called reduced-order model II. It can be observed that the proposed reduced-order model is in good accord with the small-signal model and oscillates with equal amplitude, while the conventional reduced-order model is convergent and stable, which cannot describe the instability of the system. This proves that the proposed reduced-order model is more accurate than the conventional reduced-order model.

B. Experimental Results

To further verify the analysis in this paper, the experimental tests are carried out with a three-phase grid-connected inverter with the downscaled voltage and power ratings. The configuration of the experimental setup is shown in Fig. 16. A programmable dc power supply is adopted on the dc side of the inverter to simulate the output characteristics of renewable energy. And the parameters for experiments are listed in Table II.

Fig. 17 shows the experimental results with four designed cases in Section V.A when the grid voltage drops to 0.9 p.u.. As displayed in Fig. 17 (a), (b), and (c), the dynamic response waveforms of the inverter are consistent with each other under different bandwidths of the current control loop. It implies that the variation of the current controller parameters in a large range will not significantly change the dynamics of the inverter. This proves that the dynamic of the current control loop has little effect on the system stability. Besides, Fig. 17 (a) and (d) shows the comparison of the experimental results with and without the negative feedback loop, it can be observed that the negative feedback loop increases the damping of the inverter and almost has no effect on the oscillation frequency. This indirectly proves that the positive feedback loop introduced by the network inductance will decrease the system damping while having little effect on the oscillation frequency, which is accorded with the analysis in Section IV.B. The above experimental results are consistent with the hardware-in-the-loop simulation results, which further verify the analysis of this paper.

VI. CONCLUSION

The low-frequency instability of the grid-tied inverter is mainly dominated by the slow dynamics, whereas the fast dynamics including the current control loop and network dynamic affect the behavior of the slow dynamics, which cannot be arbitrarily ignored. This paper investigates the impact of fast dynamics on the stability of the grid-tied inverter. The results

Authorized licensed use limited to: SICHUAN UNIVERSITY. Downloaded on June 06,2022 at 09:26:40 UTC from IEEE Xplore. Restrictions apply.

show that the dynamic of the current control loop has a slight effect on the stability dominated by slow dynamics, while the dynamic of the network inductance reduces the damping of the PLL especially under weak grid conditions, which plays an important role in the system stability. These analyses provide physical insight into the interactions between the fast and slow dynamics of the inverter. Additionally, considering the dynamic of the network inductance, a reduced-order model is proposed based on the impact analysis of the fast dynamics. Compared with the conventional reduced-order model, the proposed model improves accuracy without increasing complexity. On the basis of the proposed model, the difficulty of future studies focusing on the stability of power systems integrated with large-scale inverters can be greatly reduced.

APPENDIX

Expressions of K_1-K_5, $B^{\mathrm{c}}(s)$, $C^{\mathrm{L}}(s)$, and the Additional Coefficients

$$K_1 = \frac{1}{U_{\mathrm{dc0}}C}$$

$$K_2 = \frac{3}{2}U_{\mathrm{g0}}\cos\varphi_0$$

$$K_3 = U_{\mathrm{g0}}\cos\varphi_0$$

$$K_4 = -\frac{3}{2}U_{\mathrm{g0}}i_{\mathrm{d0}}\sin\varphi_0$$

$$K_5 = -\frac{3}{2}U_{\mathrm{g0}}\sin\varphi_0$$

$$B^{\mathrm{c}}(s) = \frac{2Ls^4 + K_1K_2Ls^2(k_{\mathrm{vp}}s + k_{\mathrm{vi}})}{k_{\mathrm{ip}}s + k_{\mathrm{ii}}}$$

$$C^{\mathrm{L}}(s) = -L_{\mathrm{g}}i_{\mathrm{d0}}s(k_{\mathrm{pp}}s + k_{\mathrm{pi}})$$

The mathematical expressions of $B^{\mathrm{c}}(s)$ and $C^{\mathrm{L}}(s)$ with taking resistances into consideration are as follows (a bar above the letters to show the distinction)

$$\bar{B}^{\mathrm{c}}(s) = \frac{Ls^4 + Rs^3}{k_{\mathrm{ip}}s + k_{\mathrm{ii}}} + \frac{K_1K_2Ls^2(k_{\mathrm{vp}}s + k_{\mathrm{vi}})}{(R + k_{\mathrm{ip}})s + k_{\mathrm{ii}}} + \frac{Ls^2\left[Ls^2 + (R + k_{\mathrm{ip}})s + k_{\mathrm{ii}}\right]s^2}{(k_{\mathrm{ip}}s + k_{\mathrm{ii}})\left[(R + k_{\mathrm{ip}})s + k_{\mathrm{ii}}\right]}$$

$$\bar{C}^{\mathrm{L}}(s) = -i_{\mathrm{d0}}s\frac{(RL_{\mathrm{g}} + L_{\mathrm{g}}k_{\mathrm{ip}} - R_{\mathrm{g}}L)s + L_{\mathrm{g}}k_{\mathrm{ii}}}{Ls^2 + (R + k_{\mathrm{ip}})s + k_{\mathrm{ii}}}(k_{\mathrm{pp}}s + k_{\mathrm{pi}})$$

Define $\mu = \sigma^2 + \omega_{\mathrm{n}}^2$ and $\eta = \sigma^2 - \omega_{\mathrm{n}}^2$, the mathematical expressions of d_{11}^{c}, k_{11}^{c}, d_{22}^{L} and k_{22}^{L} are as follows

$$d_{11}^{\mathrm{c}} = \frac{2L(k_{\mathrm{ip}}\mu^2 + 2k_{\mathrm{ip}}\mu\eta + 4k_{\mathrm{ii}}\sigma\eta)}{(k_{\mathrm{ii}} + k_{\mathrm{ip}}\sigma)^2 + (k_{\mathrm{ip}}\omega_{\mathrm{n}})^2} + \frac{K_1K_2L\left[2k_{\mathrm{vp}}k_{\mathrm{ip}}\mu\sigma + k_{\mathrm{vp}}k_{\mathrm{ii}}(2\eta + \mu) + k_{\mathrm{vi}}(k_{\mathrm{ip}}\mu + 2k_{\mathrm{ii}}\sigma)\right]}{(k_{\mathrm{ip}}\sigma + k_{\mathrm{ii}})^2 + (k_{\mathrm{ip}}\omega_{\mathrm{n}})^2}$$

$$k_{11}^{\mathrm{c}} = -\frac{2L(2k_{\mathrm{ip}}\sigma\mu^2 + k_{\mathrm{ii}}\mu^2 + 2k_{\mathrm{ii}}\mu\eta)}{(k_{\mathrm{ii}} + k_{\mathrm{ip}}\sigma)^2 + (k_{\mathrm{ip}}\omega_{\mathrm{n}})^2} - \frac{K_1K_2L\mu(k_{\mathrm{vp}}k_{\mathrm{ip}}\mu + 2k_{\mathrm{vp}}k_{\mathrm{ii}}\sigma + k_{\mathrm{vi}}k_{\mathrm{ii}})}{(k_{\mathrm{ip}}\sigma + k_{\mathrm{ii}})^2 + (k_{\mathrm{ip}}\omega_{\mathrm{n}})^2}$$

$$d_{22}^{\mathrm{L}} = -L_{\mathrm{g}}i_{\mathrm{d0}}(k_{\mathrm{pi}} + 2k_{\mathrm{pp}}\sigma)$$

$$k_{22}^{\mathrm{L}} = L_{\mathrm{g}}i_{\mathrm{d0}}k_{\mathrm{pp}}\mu.$$

REFERENCES

[1] B. K. Bose, "Global energy scenario and impact of power electronics in 21st century," *IEEE Trans. Ind. Electron.*, vol. 60, no. 7, pp. 2638–2651, Jul. 2013.

[2] B. Kroposki *et al.*, "Achieving a 100% renewable grid: Operating electric power systems with extremely high levels of variable renewable energy," *IEEE Power Energy Mag*, vol. 15, no. 2, pp. 61–73, Mar./Apr. 2017.

[3] S. Huang, J. Schmall, J. Conto, J. Adams, Y. Zhang, and C. Carter, "Voltage control challenges on weak grids with high penetration of wind generation: ERCOT experience," in *Proc. IEEE PES Gen. Meeting*, 2012, pp. 1–7.

[4] X. Xie, X. Zhang, H. Liu, H. Liu, Y. Li, and C. Zhang, "Characteristic analysis of subsynchronous resonance in practical wind farms connected to series-compensated transmissions," *IEEE Trans. Energy Convers.*, vol. 32, no. 3, pp. 1117–1126, Sep. 2017.

[5] C. Zou *et al.*, "Analysis of resonance between a VSC-HVDC converter and the AC grid," *IEEE Trans. Power Electron.*, vol. 33, no. 12, pp. 10157–10168, Dec. 2018.

[6] H. Liu *et al.*, "Subsynchronous interaction between direct-drive PMSG based wind farms and weak AC networks," *IEEE Trans. Power Syst.*, vol. 32, no. 6, pp. 4708–4720, Nov. 2017.

[7] M. Zhao, X. Yuan, J. Hu, and Y. Yan, "Voltage dynamics of current control time-scale in a VSC-connected weak grid," *IEEE Trans. Power Syst.*, vol. 31, no. 4, pp. 2925–2937, Jul. 2016.

[8] Y. Gu, N. Bottrell, and T. C. Green, "Reduced-order models for representing converters in power system studies," *IEEE Trans. Power Electron.*, vol. 33, no. 4, pp. 3644–3654, Apr. 2018.

[9] J. Z. Zhou, H. Ding, S. Fan, and Y. Zhang, "Impact of short-circuit ratio and phase-locked-loop parameters on the small-signal behavior of a VSC-HVDC converter," *IEEE Trans. Power Del.*, vol. 29, no. 5, pp. 2287–2296, Oct. 2014.

[10] D. Lu, X. Wang, and F. Blaabjerg, "Impedance-based analysis of DC-link voltage dynamics in voltage-source converters," *IEEE Trans. Power Electron.*, vol. 34, no. 4, pp. 3973–3985, Apr. 2019.

[11] J. Liu *et al.*, "Impact of power grid strength and PLL parameters on stability of grid-connected DFIG wind farm," *IEEE Trans. Sustain. Energy*, vol. 11, no. 1, pp. 545–557, Jan. 2020.

[12] H. Yuan, X. Yuan, and J. Hu, "Modeling of grid-connected VSCs for power system small-signal stability analysis in DC-link voltage control timescale," *IEEE Trans. Power Syst.*, vol. 32, no. 5, pp. 3981–3991, Sep. 2017.

[13] Y. Huang, X. Yuan, J. Hu, P. Zhou, and D. Wang, "DC-bus voltage control stability affected by AC-bus voltage control in VSCs connected to weak AC grids," *IEEE J. Emerg. Sel. Topics Power Electron.*, vol. 4, no. 2, pp. 445–458, Jun. 2016.

[14] D. Wang, L. Liang, L. Shi, J. Hu, and Y. Hou, "Analysis of modal resonance between PLL and DC-link voltage control in weak-grid tied VSCs," *IEEE Trans. Power Syst.*, vol. 34, no. 2, pp. 1127–1138, Mar. 2019.

[15] J. Wang, J. D. Yan, L. Jiang, and J. Zou, "Delay-dependent stability of single-loop controlled grid-connected inverters with LCL filters," *IEEE Trans. Power Electron.*, vol. 31, no. 1, pp. 743–757, Jan. 2016.

[16] X. Guo, Z. Lu, B. Wang, X. Sun, L. Wang, and J. M. Guerrero, "Dynamic phasors-based modeling and stability analysis of droop-controlled inverters for microgrid applications," *IEEE Trans. Smart Grid*, vol. 5, no. 6, pp. 2980–2987, Nov. 2014.

[17] P. Vorobev, P. Huang, M. A. Hosani, J. L. Kirtley, and K. Turitsyn, "High-fidelity model order reduction for microgrids stability assessment," *IEEE Trans. Power Syst.*, vol. 33, no. 1, pp. 874–887, Jan. 2018.

[18] W. Du, X. Chen, and H. Wang, "PLL-induced modal resonance of grid-connected PMSGs with the power system electromechanical oscillation modes," *IEEE Trans. Sustain. Energy*, vol. 8, no. 4, pp. 1581–1591, Oct. 2017.

[19] J. Hu, Q. Hu, B. Wang, H. Tang, and Y. Chi, "Small signal instability of PLL-synchronized type-4 wind turbines connected to high-impedance AC grid during LVRT," *IEEE Trans. Energy Convers.*, vol. 31, no. 4, pp. 1676–1687, Dec. 2016.

Authorized licensed use limited to: SICHUAN UNIVERSITY. Downloaded on June 06,2022 at 09:26:40 UTC from IEEE Xplore. Restrictions apply.

[20] S. V. Iyer, M. N. Belur, and M. C. Chandorkar, "A generalized computational method to determine stability of a multi-inverter microgrid," *IEEE Trans. Power Electron.*, vol. 25, no. 9, pp. 2420–2432, Sep. 2010.
[21] J. Hu, H. Yuan, and X. Yuan, "Modeling of DFIG-based WTs for small-signal stability analysis in DVC timescale in power electronized power systems," *IEEE Trans. Energy Convers.*, vol. 32, no. 3, pp. 1151–1165, Sep. 2017.
[22] M. Rasheduzzaman, J. A. Mueller, and J. W. Kimball, "Reduced-order small-signal model of microgrid systems," *IEEE Trans. Sustain. Energy*, vol. 6, no. 4, pp. 1292–1305, Oct. 2015.
[23] Z. Yuan, Z. Du, C. Li, and T. An, "Dynamic equivalent model of VSC based on singular perturbation," *IET Gener., Transmiss., Distrib.*, vol. 10, no. 14, pp. 3413–3422, 2016.
[24] S. Liao *et al.*, "A novel dynamic aggregation modeling method of grid-connected inverters: Application in small-signal analysis," *IEEE Trans. Sustain. Energy*, vol. 10, no. 3, pp. 1554–1564, Jul. 2019.
[25] H. Wu and X. Wang, "Design-oriented transient stability analysis of PLL-synchronized voltage-source converters," *IEEE Trans. Power Electron.*, vol. 35, no. 4, pp. 3573–3589, Apr. 2020.
[26] H. Zhang, Z. Liu, S. Wu, and Z. Li, "Input impedance modeling and verification of single-phase voltage source converters based on harmonic linearization," *IEEE Trans. Power Electron.*, vol. 34, no. 9, pp. 8544–8554, Sep. 2019.
[27] X. Wang, J. Yao, J. Pei, P. Sun, H. Zhang, and R. Liu, "Analysis and damping control of small-signal oscillations for VSC connected to weak AC grid during LVRT," *IEEE Trans. Energy Convers.*, vol. 34, no. 3, pp. 1667–1676, Sep. 2019.
[28] X. Wang, F. Blaabjerg, and W. Wu, "Modeling and analysis of harmonic stability in an AC power-electronics-based power system," *IEEE Trans. Power Electron.*, vol. 29, no. 12, pp. 6421–6432, Dec. 2014.
[29] L. Harnefors, M. Bongiorno, and S. Lundberg, "Input-admittance calculation and shaping for controlled voltage-source converters," *IEEE Trans. Ind. Electron.*, vol. 54, no. 6, pp. 3323–3334, Dec. 2007.
[30] F. P. Demello and C. Concordia, "Concepts of synchronous machine stability as affected by excitation control," *IEEE Trans. Power App. Syst.*, vol. PAS-88, no. 4, pp. 316–329, Apr. 1969.

Pan Yu received the B.Eng. degree from the School of Mechatronics Engineering, University of Electronic Science and Technology of China, Chengdu, China, in 2017. He is currently working toward the Ph.D. degree in electrical engineering with the School of Electrical and Automation, Wuhan University, Wuhan, China.

His research interests include modeling, analysis and control of power electronic systems.

Zhen Tian (Member, IEEE) received the B.S. degree from Wuhan University, Wuhan, China, in 2014 and the Ph.D. degree from Shanghai Jiao Tong University, Shanghai, China, in 2019.

During 2017–2019, he was a Visiting Scholar with the Department of Electrical and Computer Engineering, Illinois Institute of Technology, Chicago, IL, USA. He is currently a Postdoctoral Researcher with the School of Electrical Engineering and Automation, Wuhan University. His research interests include modeling, control and stability analysis of power converters, microgrids and power-electronics-enabled power systems.

Xiaoming Zha (Member, IEEE) was born in Huaining, Anhui Province, China, in 1967. He received the B.S., M.S., and Ph.D. degrees in electrical engineering from Wuhan University, Wuhan, China, in 1989, 1992, and 2001, respectively. From 2001 to 2003, he was a Postdoctoral Fellow with the University of Alberta, Canada. Since 1992, he has been a Faculty Member of Wuhan University, and became a Professor in 2003. He is currently the Deputy Dean with the School of Electrical Engineering, Wuhan University.

His research interests include power electronic converter, the application of power electronics in smart grid and renewable energy generation, the analysis and control of microgrid, the analysis and control of power quality, and frequency control of high-voltage high-power electric motors.

Jianjun Sun (Member, IEEE) was born in 1975. He received the B.Eng., M.Eng., and Ph.D. degrees in electrical engineering from Wuhan University, Wuhan, China, in 1997, 2000, and 2007, respectively.

He is currently with the School of Electrical Engineering, Wuhan University, as a Full Professor and the Deputy Director of Motor and Power Electronics Center. His current research interests include modeling and analysis of power-electronic system and microgrid.

Peijun Zhong received the B.Eng. degree in automation from Xiangtan University, Xiangtan, China, in 2017. He is currently working toward the Ph.D. degree in electrical engineering with the School of Electrical and Automation, Wuhan University, Wuhan, China.

His research interests mainly include parameter measurement analysis and application of power-electronics-enabled power systems.

Meng Huang (Member, IEEE) received the B.Eng. and M.Eng. degrees from the Huazhong University of Science and Technology, Wuhan, China, in 2006 and 2008, respectively, and the Ph.D. degree from Hong Kong Polytechnic University, Hong Kong, in 2013.

He is currently an Associate Professor with the School of Electrical Engineering, Wuhan University, Wuhan, China. His research interests include nonlinear analysis of power converters and power electronics reliability.

Authorized licensed use limited to: SICHUAN UNIVERSITY. Downloaded on June 06,2022 at 09:26:40 UTC from IEEE Xplore. Restrictions apply.